Computation of Shock Wave Reflection by Circular Cylinders

J. Y. Yang,* Yen Liu,† and Harvard Lomax‡
NASA Ames Research Center, Moffett Field, California

The nonstationary shock wave diffraction patterns generated by a blast wave impinging on a circular cylinder are numerically simulated using a second-order hybrid upwind method for solving the two-dimensional inviscid compressible Euler equations of gasdynamics. The diffraction was followed through about 6 radii of travel of the incident shock past the cylinder. A broad range of incident shock Mach numbers are covered. The complete diffraction patterns, including the transition from regular to Mach reflection, trajectory of the Mach triple point, and the complex shock-on-shock interaction at the wake region resulting from the Mach shocks collision behind the cylinder are reported in detail. Pressure-time history and various contour plots are also included. Comparison between the work of Bryson and Gross, which included both experimental schlieren pictures and theoretical calculations using Whitham's ray/shock theory, and results of the present finite-difference computation indicate good agreement in every aspect except for some nonideal gas and viscous effects that are not accounted for by the Euler equations.

Introduction

THE problem of the propagation of shock waves over circular cylinders has been studied experimentally and analytically by many investigators.[1,3,4] When a planar shock wave propagates and encounters a cylinder, it first experiences a head-on collision and immediately reflects into a two-shock system referred to as regular reflection. The confluence point travels along the cylinder surface and, as the shock wave propagates up the cylinder surface, the reflecting wedge angle at the reflection point decreases until the Mach effect occurs, i.e., until the regular reflection changes into a Mach reflection. Here a new shock, called a Mach shock, is formed; it can be recognized by the three-shock system. The confluence point now leaves the surface and becomes a triple point. A slipstream originates from the triple point and eventually curls up to form a vortex. As the incident shock propagates further downstream, some complex shock-shock interactions occur as the Mach shocks collide behind the cylinder. An illustration and definition of shock structures for a typical shock diffraction around a circular cylinder will be shown using a series of computed isopycnics.

In the past, many experimental and analytical investigations have been conducted to study oblique shock wave reflection problems. One of the main issues concerning shock reflection is the establishment of the criteria for predicting the transition between regular and Mach reflections. Several approximate theories have been developed to analyze and predict such transition and the trajectory of the triple point. The best known theory for predicting the shock-shock interaction problem is the ray-shock theory of Whitham.[2]

An extensive theoretical calculation of the shock diffraction around a cylinder that employs Whitham's theory was given by Bryson and Gross.[1] In Ref. 1, a series of schlieren pictures taken from a shock tube experiment were presented to check the accuracy of the theory and to illustrate the complex diffraction flow patterns. Many details of the flowfield are revealed. Similar studies were also presented by Heilig.[3] Reference 3 provides a very useful data base against which to validate and assess the accuracy of computer codes and from which to extend the applicability of such codes to other complex problems that may not be easily studied by experiments due to such limitations as interference effects.

On the other hand, because of recent improvements in numerical techniques for solving the Euler equations and the increased power of supercomputers, major advances have been made in the field of numerical simulation of oblique shock wave reflection. A survey on the application of numerical solutions of two-dimensional gasdynamics with strong shocks in simple geometries producing self-similar solution was given by Woodward and Collela.[5] Fine resolution of the complicated flowfields created by shock wave/wedge interaction was obtained with a sufficiently fine computational grid and with reasonable computing time on a supercomputer. Some demonstrations of such computational capability for simulating such flows can be found in Refs. 6 and 7.

In this paper, we numerically simulate the complicated flowfields generated by a shock wave impinging on a circular cylinder by solving the time-dependent, compressible Euler equations in the general curvilinear coordinate systems. The main purposes in this study are twofold: 1) to solve the truly unsteady flowfield of a shock diffracted by a circular cylinder and to compare the results directly with those found by experiments; this allows us to evaluate the present numerical method for predicting shock-on-shock interaction in unsteady gas dynamics; and 2) to provide detailed flowfield data by means of various contour plots and pressure-time histories. Such data are not easily obtainable in laboratory experiments.

In the following, we first outline the numerical method and then show some results of our calculations. Comparison with experimental results are included.

Governing Equations

The conversation equations of the two-dimensional unsteady gasdynamics, neglecting the effects of viscosity and heat transfer, in general curvilinear coordinate systems (ξ, η) can be written as follows:

$$\partial_\tau Q + \partial_\xi F + \partial_\eta G = 0 \tag{1}$$

Presented as Paper 86-0272 at the AIAA 24th Aerospace Sciences Meeting, Reno, NV, Jan. 6–9, 1986; received Feb. 7, 1986; revision received Aug. 12, 1986.

*NRC Research Associate, Computational Fluid Dynamics Branch; currently Associate Professor, Institute of Applied Mechanics, National Taiwan University, Taipei, Taiwan. Member AIAA.

†NRC Research Associate, Computational Fluid Dynamics Branch. Member AIAA.

‡Research Scientist, Computational Fluid Dynamics Branch. Fellow AIAA.

where

$$Q = \hat{Q}/J$$

$$F = \left(\xi_t \hat{Q} + \xi_x \hat{F} + \xi_y \hat{G}\right)/J$$

$$G = \left(\eta_t \hat{Q} + \eta_x \hat{F} + \eta_y \hat{G}\right)/J$$

and where the metric Jacobian is

$$J = \xi_x \eta_y - \xi_y \eta_x$$

In the Cartesian coordinates, the conservative state vector is

$$\hat{Q} = (\rho, \rho u, \rho v, e)^T$$

and the flux vectors are

$$\hat{F} = \left[\rho u, \rho u^2 + p, \rho uv, u(e+p)\right]^T$$

$$\hat{G} = \left[\rho v, \rho vu, \rho v^2 + p, v(e+p)\right]^T$$

Here ρ is the gas density, u, v the gas velocity components, e the internal energy, and p the gas pressure. The pressure p is related to ρ, u, v, and e for an ideal gas by

$$p = (\gamma - 1)\left[e - 0.5\rho(u^2 + v^2)\right] \tag{2}$$

where γ is the specific heats ratio. Equation (1) is a hyperbolic system of conservation laws; hence, both hyperbolicity and conservation law properties of the system can be utilized to construct a solution procedure for solving them.

Due to the hyperbolicity of Eq. (1), the Jacobian coefficient matrix $A_\xi = \partial F/\partial Q$ of the transformed equations has real eigenvalues,

$$a_1 = U, \quad a_2 = U + c_\xi, \quad a_3 = U, \quad a_4 = U - c_\xi \tag{3}$$

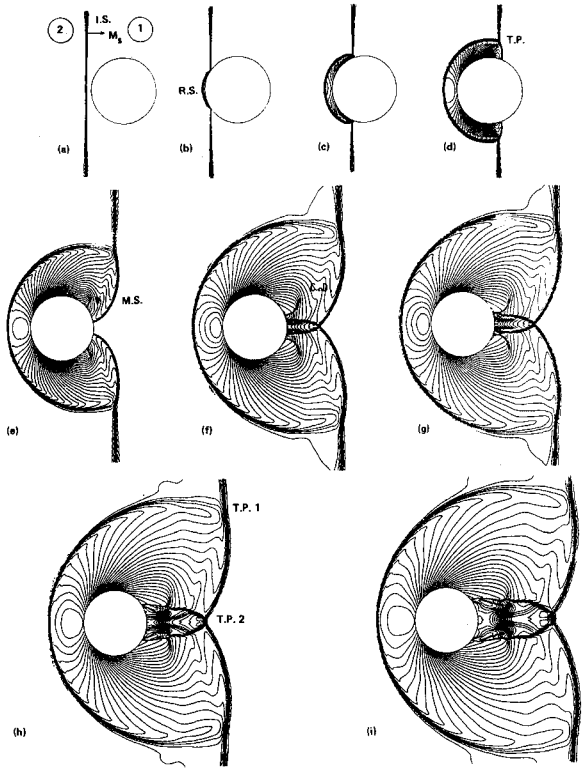

Fig. 1 Computed isopycnics of shock diffraction on a cylinder at $M_s = 2.81$ (I.S. = incident shock, R.S. = reflected shock, M.S. = Mach shock, C.D. = contact discontinuity, T.P. = triple point, V = vortex).

with

$$U = \xi_t + \xi_x u + \xi_y v \quad \text{and} \quad c_\xi = c\sqrt{\xi_x^2 + \xi_y^2}$$

where $c = \sqrt{\gamma p/\rho}$ is the speed of sound. Similarly, the eigenvalues of $B_\eta = \partial G/\partial Q$ are

$$b_1 = V, \quad b_2 = V, \quad b_3 = V + c_\eta, \quad b_u = V - c_\eta$$

with

$$V = \eta_t + \eta_x u + \eta_y v \quad \text{and} \quad c_\eta = c\sqrt{\eta_x^2 + \eta_y^2}$$

One can find similarity transformation matrices T_ξ and T_η such that

$$T_\xi^{-1} A_\xi T_\xi = \Lambda_\xi = \text{diag}\{a_\ell\}$$

$$T_\eta^{-1} B_\eta T_\eta = \Lambda_\eta = \text{diag}\{b_\ell\} \tag{4}$$

The eigenvalues of the hyperbolic system provide the wave propagation information via the theory of characteristics. Their signs indicate the direction-biased difference formula to be used for the finite-difference approximation when solving Eq. (1).

Described in the following section is a finite-difference numerical method of second-order accuracy in time and space that combines both the characteristic and conservation features of Eq. (1).

Numerical Algorithm: A Hybrid Approach

First, let us define a computational mesh system (ξ_j, η_k) with mesh sizes $\Delta\xi$ and $\Delta\eta$. Let $Q^n_{j,k}$ denote the value of Q at time level $n\Delta\tau$ and at position $(j\Delta\xi, k\Delta\eta)$.

An explicit, conservative, finite-difference scheme for Eq. (1) can be expressed in terms of numerical fluxes F^N and G^N as

$$\frac{Q^{n+1}_{j,k} - Q^n_{j,k}}{\Delta\tau} + \frac{F^N_{j+\frac{1}{2},k} - F^N_{j-\frac{1}{2}k}}{\Delta\xi} + \frac{G^N_{j,k+\frac{1}{2}} - G^N_{j,k-\frac{1}{2}}}{\Delta\eta} = 0 \tag{5}$$

Using dimensional splitting, the solution procedure becomes locally one-dimensional and can be represented as

$$Q^{n+2}_{j,k} = L_\xi(\Delta\tau)\, L_\eta(\Delta\tau)\, L_\eta(\Delta\tau)\, L_\xi(\Delta\tau)\, Q^n_{j,k} \tag{6}$$

In the following, only the L_ξ operator is described in detail. A similar expression can be given for the L_η operator.

For the L_ξ operator in the ξ direction, we have

$$L_\xi Q^n_{j,k} = Q^*_{j,k} = Q^n_{j,k} - \lambda_\xi\left(F^N_{j+\frac{1}{2},k} - F^N_{j-\frac{1}{2},k}\right) \tag{7}$$

where $\lambda_\xi = \Delta\tau/\Delta\xi$ and $F^N_{j+\frac{1}{2},k}$ is the numerical flux remaining to be defined. In this study, we adopt a hybrid approach that combines the flux vector splitting methods,[8,9] the modified flux method,[10] and the characteristic flux difference splitting method.[11]

The numerical flux $F^N_{j+\frac{1}{2},k}$ is given by

$$F^N_{j+\frac{1}{2},k} = F^n_{j+1,k} - \Delta_{j+\frac{1}{2},k} F^+ + \frac{1}{\lambda_\xi}\left(E_{j+1,k} - \hat{A}^+_{\xi_{j+\frac{1}{2},k}} \Delta_{j+\frac{1}{2},k} E\right) \tag{8a}$$

$$= F^n_{j,k} + \Delta_{j+\frac{1}{2},k} F^- + \frac{1}{\lambda_\xi}\left(E_{j,k} + \hat{A}^-_{\xi_{j+\frac{1}{2},k}} \Delta_{j+\frac{1}{2},k} E\right) \tag{8b}$$

with $\Delta_{j+\frac{1}{2}}() = ()_{j+1} - ()_j$.

In Eq. (8), F presents the original flux vector: $F^\pm$ the split flux vectors given by either Ref. 8 or 9, E a modified flux

vector similar to the one given in Ref. 10, and $\hat{A}_\xi^\pm$ the split "normalized" Jacobian coefficient matrices defined in Ref. 11.

The $\hat{A}_\xi^\pm$ is closely related through

$$T_\xi^{-1}\hat{A}_\xi^\pm T_\xi = \hat{\Lambda}_\xi^\pm = \text{diag}\{\hat{a}_\ell^\pm\}, \qquad \hat{a}_\ell^\pm = \frac{1 \pm \text{sgn}(a_\ell)}{2} \tag{9}$$

The value of E at point j,k is $E_{j,k} = (e_1, e_2, e_3, e_4)^T_{j,k}$ and its ℓ components is given by

$$e_{\ell_{j,k}} = 0, \quad \text{if} \quad \tilde{e}_{\ell_{j+\frac{1}{2},k}}\tilde{e}_{\ell_{j-\frac{1}{2},k}} \le 0$$

$$= s_{\ell_{j+\frac{1}{2},k}} \min\left(|\tilde{e}_{\ell_{j+\frac{1}{2},k}}|, |\tilde{e}_{\ell_{j-\frac{1}{2},k}}|\right), \quad \text{otherwise} \tag{10}$$

where $\tilde{e}_{\ell_{j+\frac{1}{2},k}}(\ell = 1,2,3,4)$ are components of the following column vector:

$$\tilde{E}_{j+\frac{1}{2},k} = \frac{\lambda_\xi}{2}|A_{\xi_{j+\frac{1}{2},k}}|\left(I - \lambda_\xi|A_{\xi_{j+\frac{1}{2},k}}|\right)\Delta_{j+\frac{1}{2},k}Q \tag{11}$$

and

$$s_{\ell_{j+\frac{1}{2},k}} = \text{sgn}\left(\tilde{e}_{\ell_{j+\frac{1}{2},k}}\right) \tag{12}$$

Other forms of the modified flux vectors can also be found in Refs. 12–14.

The $|A_\xi|$ in Eq. (11) is given by

$$|A_\xi| = T_\xi \,\text{diag}\{|a_\ell|\}\, T_\xi^{-1} \tag{13}$$

In the following, the split flux vectors defined in Ref. 9 are used (see also Ref. 15). The flux is split according to the contravariant Mach number in the ξ direction, defined as $M_\xi = U/c_\xi$.

For $|M_\xi| < 1$,

$$F^\pm = f_\rho^\pm\left(1, \frac{\tilde{\xi}_x(-U_\xi \pm 2c)}{\gamma} + u, \frac{\tilde{\xi}_y(-U_\xi \pm 2c)}{\gamma} + v, \frac{\left[(\gamma-1)U_\xi \pm 2c\right]^2}{2(\gamma^2-1)} + \frac{V_\xi^2}{2}\right)^T \tag{14}$$

where

$$f_\rho^\pm = \pm\frac{\rho c}{4}(M_\xi \pm 1)^2|\nabla\xi|/J$$

$$U_\xi = U/|\nabla\xi|, \quad V_\xi = (v\xi_x - u\xi_y)/|\nabla\xi|$$

$$\tilde{\xi}_x = \xi_x/|\nabla\xi|$$

For $|M_\xi| \ge 1$,

$$F^+ = F, \quad F^- = 0, \quad M_\xi \ge +1 \tag{15a}$$

$$F^+ = 0, \quad F^- = F, \quad M_\xi \le -1 \tag{15b}$$

Boundary and Initial Conditions

The integration scheme of Eq. (7) is for the interior points. At the cylinder surface ($k = 1$) and outer boundary ($k = K$), one has

$$Q_{j,1}^* = Q_{j,1}^n - \lambda_\eta \hat{B}_{j,3/2}^-(G_{j,2} - G_{j,1}) \tag{16a}$$

and

$$Q_{j,K}^* = Q_{j,K}^n - \lambda_\eta \hat{B}_{j,K-\frac{1}{2}}^+(G_{j,K} - G_{j,K-1}) \tag{16b}$$

Additional conditions are needed to supplement Eq. (16a) in order to update the state variables Q on the cylinder surface ($k = 1$). These are furnished by the Riemann invariants

$$V_\eta^{n+1} - \frac{2c^{n+1}}{(\gamma-1)} = V_\eta^* - \frac{2c^*}{(\gamma-1)} \tag{17a}$$

$$\frac{p^{n+1}}{(\rho^{n+1})^\gamma} = \frac{p^*}{(\rho^*)^\gamma} \tag{17b}$$

$$U_\eta^{n+1} = U_\eta^* \tag{17c}$$

and the surface tangency condition

$$V_\eta^{n+1} = 0 \tag{17d}$$

where $V_\eta = V/|\nabla\eta|$ and $U_\eta = (\eta_y u - \eta_x v)/|\nabla\eta|$.

Equation (17) gives one the four equations to solve for the state variables $Q_{j,1}^{n+1}$ at the new time level.

In the ξ direction, one integrates the equations from $j = 1$ to $j = J - 1$ and resets the flow quantities at line $j = J$ identical to those at line $j = 1$, where these two grid lines overlap (the line passing through the origin of the cylinder and the rear stagnation point).

The initial position of the incident shock is arbitrarily located at certain distance to the left of the cylinder (Fig. 1a). The conditions ahead of (state 1) and behind (state 2) a moving shock related by

$$\frac{p_2}{p_1} = \frac{2\gamma M_s^2 - (\gamma-1)}{(\gamma+1)} \tag{18a}$$

$$\frac{\rho_2}{\rho_1} = \frac{\Gamma(p_2/p_1) + 1}{\Gamma + (p_2/p_1)} \tag{18b}$$

$$u_2 = M_s\left[1 - \frac{(\gamma-1)M_s^2 + 2}{(\gamma+1)M_s^2}\right]c_1 \tag{18c}$$

where $\Gamma = (\gamma+1)/(\gamma-1)$ and $c_1 = (\gamma p_1/\rho_1)^{\frac{1}{2}}$.

Initially, when $\tau = 0$, the conditions at state 1 are $\rho_1 = 1$, $p_1 = 1$, $u_1 = 0$, and $v_1 = 0$ and conditions at state 2 are given by Eq. (18) with an assigned value of M_s and a given value of γ for a particular gas. Moving shock relations are applied on both sides of the incident shock and the consequent movement of the shock is simulated without imposing any explicit equation of motion for the incident shock.

Results and Discussion

A series of calculations covering a wide range of incident shock Mach numbers were carried out to study the transient shock wave diffraction phenomena produced by a blast wave impinging on a circular cylinder. In the following, results for two different incident shock Mach numbers are reported. A simple cylindrical grid system was used, consisting of 361 rays (equally spaced with 1 deg angle) around the cylinder (ξ direction) and 101 circles (slightly stretched with $\Delta r_{\min} = 0.01$) between the cylinder surface and the outer boundary (η direction). The diameter of the cylinder is 1 and the distance between the origin of the cylinder and the outer boundary is 5. The shock tube test gas was air and the equation of state was chosen to be a perfect (frozen) gas with $\gamma = 1.4$. At high incident shock Mach numbers, dissociation and ionization of gas may occur and real-gas effects such as chemical equilibrium or nonequilibrium should be considered. In such circumstances, both the equation of state given by Eq. (2) and the initial starting conditions defined by Eq. (18) should be modified accordingly. In all calculations, a Courant number of 0.99 was used.

First, we report the results for the case of $M_s = 2.81$ and $\gamma = 1.4$, which we compare directly with the experimental and

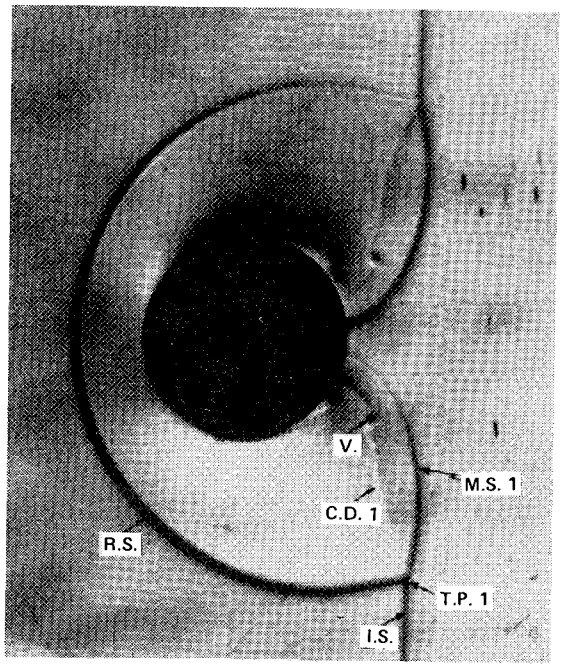

a) Experimental schlieren photograph (from Ref. 1).

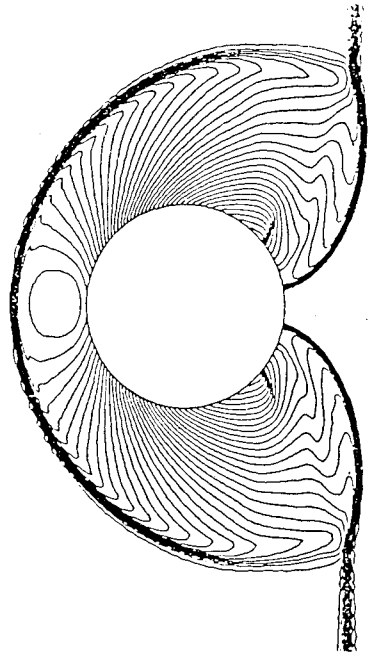

b) Computed isopycnics.

Fig. 2 Comparison for early shock diffraction on a cylinder at $M_s = 2.81$.

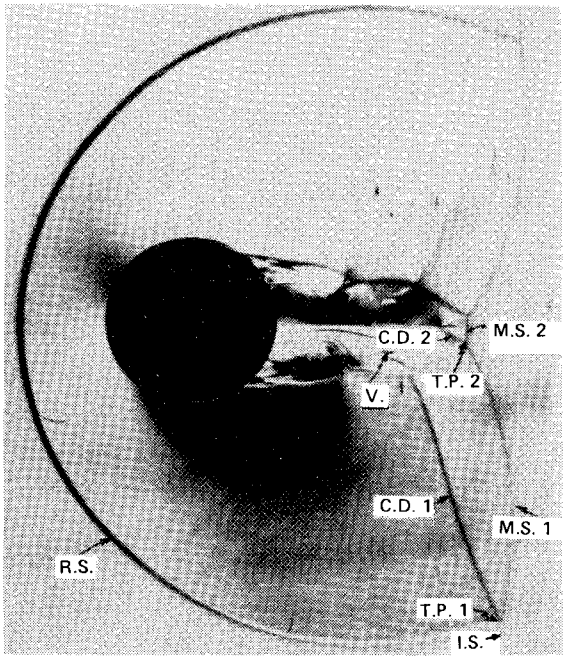

a) Experimental schlieren photograph (from Ref. 1).

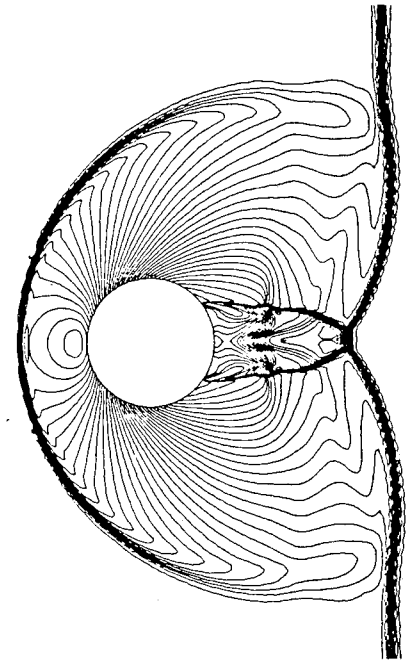

b) Computed isopycnics.

Fig. 3 Comparison for later shock diffraction on cylinder at $M_s = 2.81$.

analytical results of the ray-shock theory reported in Ref. 1. This is in order to check the present numerical method. In Fig. 1, the computed isopycnics are shown for flow with $M_s = 2.81$ at a series of times. In Fig. 1a, the incident shock is about to hit the cylinder surface and the density contours give a reasonable representation of the flow, which at this moment is constant on either side of the moving shock. Figs. 1b–1i show the subsequent development of the diffraction process that covers regular reflection, transition to Mach reflection, the Mach shocks collision at the wake, and the complex shock-on-shock interaction. The primary incident shock (I.S.), reflected bow shock (R.S.), Mach shock (M.S.), contact discontinuity (C.D.), and vortex (V) can be easily identified. Downstream of the cylinder wake, complicated flow interaction resulting in Mach shocks, second contact discontinuities, and triple point were well captured (e.g., see Fig. 1i).

The experimental schlieren pictures of Bryson and Gross[1] are duplicated and shown together with the corresponding computed density contours in Figs. 2 and 3, respectively, at two different times. Except for viscous effects, such as boundary-layer separation and its interaction with the reflected Mach shock at the wake, most of the flow features are well simulated.

The pressure-time history of the diffraction process at several positions on the cylinder surface are shown in Fig. 4. This is important for the determination of pressure loading. The trajectory of the Mach shock triple point is plotted in Fig. 5 for the case of $M_s = 2.81$ and $\gamma = 1.4$. One-half of the symmetrical diffraction pattern is shown. The pressure at the rear stagnation point experienced a sudden jump after the two Mach shocks collide. The transition point is located approximately 42 deg from the front stagnation point.

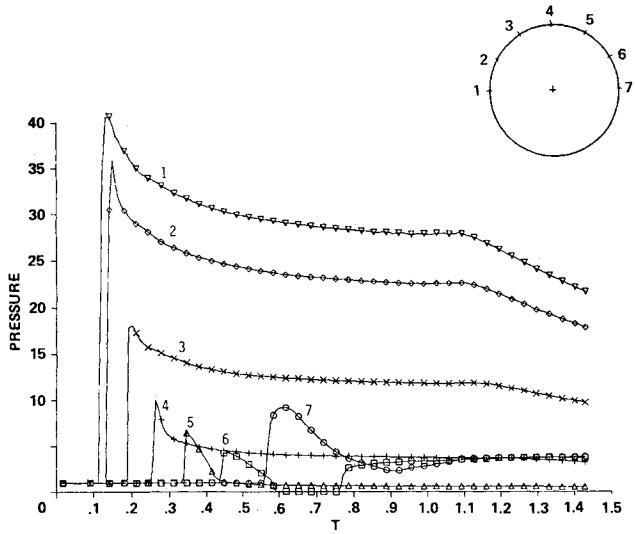

Fig. 4 Pressure-time history at $M_s = 2.81$. Pressure distribution shown at several locations on the cylinder: 1, front stagnation point; 2–6, every 30 deg; 7, rear stagnation point.

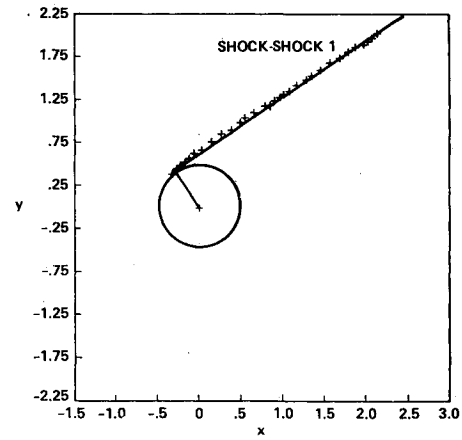

Fig. 5 Trajectories of the Mach shock triple point for shock diffraction on a cylinder at $M_s = 2.81$; Mach reflection begins between 40 and 50 deg from the front stagnation point.

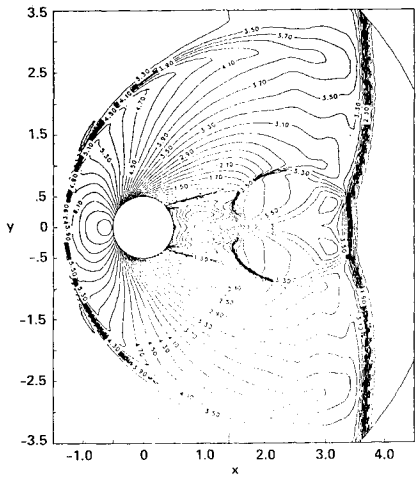

a) Density contours.

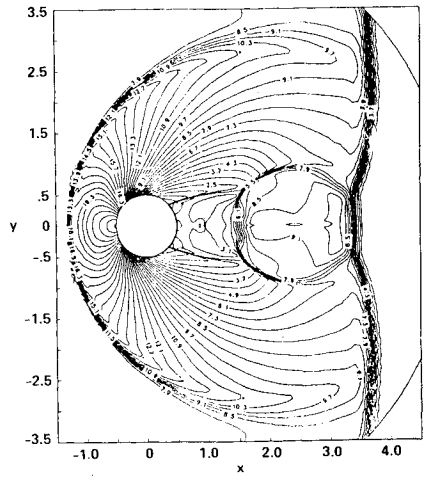

b) Pressure contours.

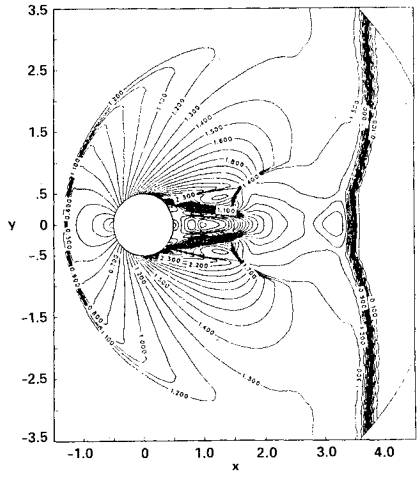

c) Mach number contours.

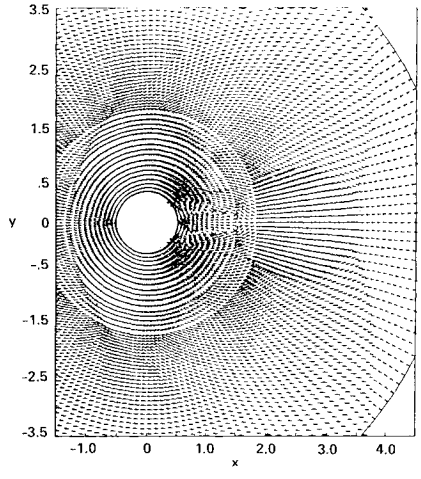

d) Velocity vectors.

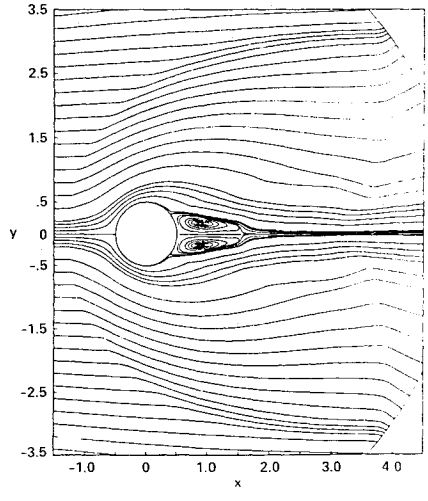

e) Streamlines.

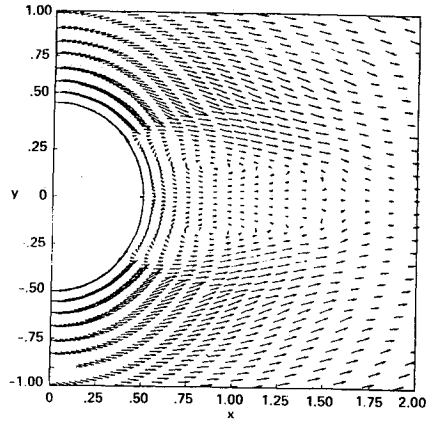

f) Enlarged view of Fig. 6d.

Fig. 6 Inviscid flowfields of shock diffraction around a circular cylinder at $M_s = 2.81$.

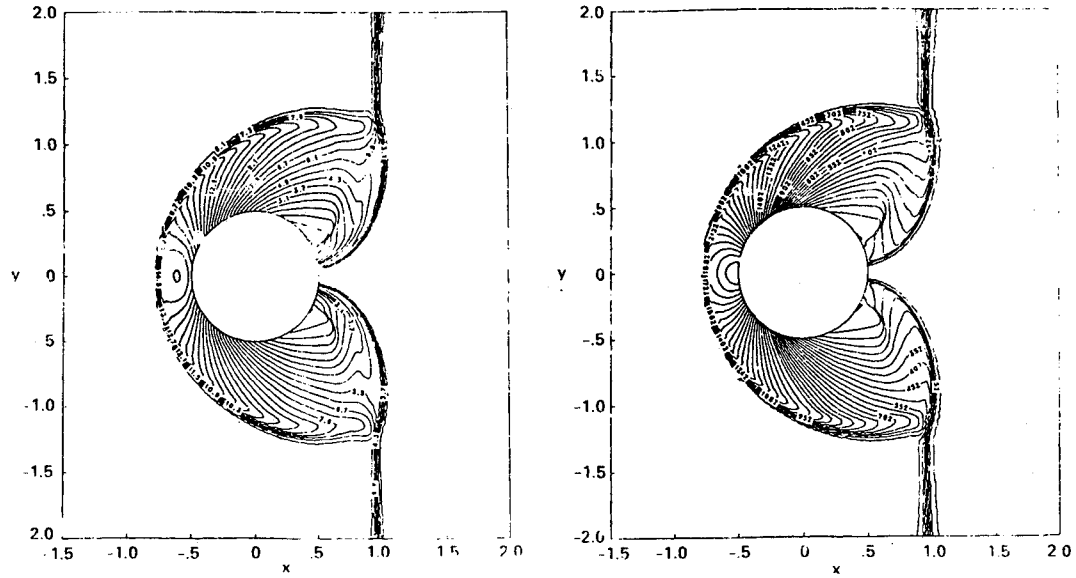

a) Density contours. b) Pressure contours.

Fig. 7 Early shock diffraction on a cylinder at $M_s = 20$.

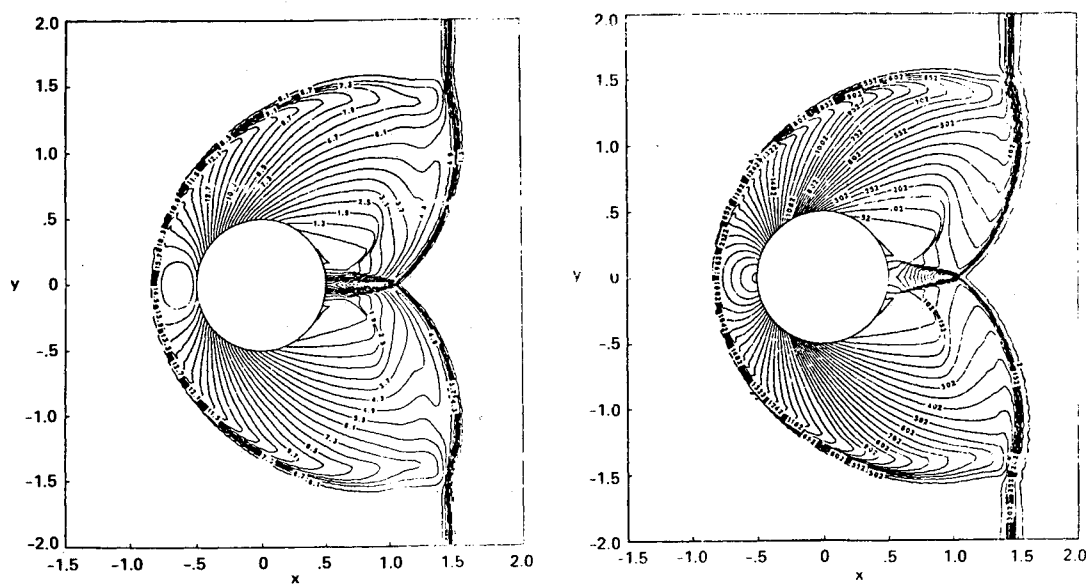

a) Density contours. b) Pressure contours.

Fig. 8 Late shock diffraction on a cylinder at $M_s = 20$.

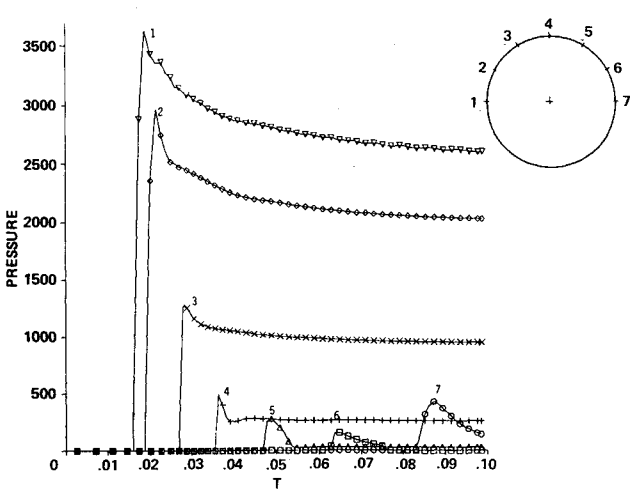

Fig. 9 Pressure-time history at $M_s = 20$. Pressure distribution shown at several location on the cylinder: 1, front stagnation point; 2–6, every 30 deg; 7, rear stagnation point.

In general, good agreement are found in terms of triple-point locus, vortex locus, and the position of the transition point from regular to Mach reflection. Note that the flow patterns are very symmetric and no vertex shedding is observed. Additional information such as various contour plots, velocity vectors, and streamlines are shown in Fig. 6 to assist the analysis of the flowfield. The separation point (at around 45 deg from the rear stagnation point) and the vortex pair are clearly shown in the streamline plot.

Finally, in Figs. 7 and 8, we also report results for the case of $M_s = 20$ and $\gamma = 1.4$ at two different times. Flow patterns similar to the case of $M_s = 2.81$ are observed. The pressure loading is much more severe in this case, as shown in Fig. 9.

Conclusions

The unsteady inviscid flowfields generated by a planar shock wave impinging on a circular cylinder have been numerically simulated by using a hybrid second-order upwind finite-difference scheme for solving the unsteady compressible Euler equations. Comparison with the experimental results of

Bryson and Gross[1] shows good agreement in every inviscid aspect of the flow phenomenon.

Detailed flow information is provided on quantities such as pressure-time history, velocity vectors, pressure contours, and quantities not easily obtainable by experiments.

Based on the present study, it is concluded that time-dependent, two-dimensional shock-on-shock interaction problems can be adequately and economically simulated using a numerical approach and that the method can be considered as an alternative to shock tube experiments, particularly when the experiments are subjected to the limitations of the interference effects.

Acknowledgments

The authors would like to thank A. E. Bryson of Stanford University for providing the experimental schlieren photographs used for comparison in this study and Pieter Buning of NASA Ames Research Center for using his PLOT3D graphic package.

References

[1]Bryson, A.E. and Gross, R.W.F., "Diffraction of Strong Shocks by Cones, Cylinders, and Spheres," *Journal of Fluid Mechanics*, Vol. 10, 1961, pp. 1–16.

[2]Whitham, G.B., "A New Approach to Problems of Shock Dynamics, Part I: Two-Dimensional Problems," *Journal of Fluid Mechanics*, Vol. 2., 1957, pp. 145–171.

[3]Heilig, W.H., "Diffraction of a Shock Wave by a Cylinder," *The Physics of Fluids*, Supp. I, 1960, pp. I—154–157.

[4]Ben-Dor, G. and Takayama, K., "Analytical Prediction of the Transition from Mach to Regular Reflection over Cylindrical Concave Wedges," *Journal of Fluid Mechanics*, Vol. 158, 1985, pp. 365–380.

[5]Woodward, P.R. and Collela, P., "The Numerical Simulation of Two-Dimensional Fluid Flow with Strong Shocks," *Journal of Computational Physics*, Vol. 51, 1984, pp. 115–173.

[6]Colella, P. and Glaz, H.M., "Computation of Shock Reflection in Gases," *Proceedings of 9th International Conference on Numerical Methods in Fluid Dynamics*, Saclay, France, 1984.

[7]Glaz, H.M., Colella, P., Glass, I.I., and Deschambault, R.L., "A Numerical Study of Oblique Shock-Wave Reflections with Experimental Comparisons," *Proceedings of the Royal Society of London*, Vol. A 398, 1985, pp. 117–140.

[8]Steger, J.L. and Warming, R.F., "Flux Vector Splitting of the Inviscid Gasdynamic Equations with Application to Finite Difference Methods," *Journal of Computational Physics*, Vol. 40, 1981, pp. 263–293.

[9]van Leer, B., "Flux-Vector Splitting for the Euler Equations," *Lecture Notes in Physics*, Vol. 170, 1982, pp. 507–512.

[10]Harten, A., "High Resolution Schemes for Hyperbolic Conservation Laws," *Journal of Computational Physics*, Vol. 49, 1983, pp. 357–393.

[11]Yang, J.Y., "A Characteristic Flux Difference Splitting Method for Hyperbolic Systems of Conservation Laws," Ph.D. Dissertation, Stanford University, Stanford, CA, March 1983.

[12]Yang, J.Y., "Numerical Solution of the Two Dimensional Euler Equations by Second-Order Upwind Difference Schemes," AIAA Paper 85-0292, 1985.

[13]Yang, J.Y., Lombard, C.K., and Bershader, D., "Computation of Nonstationary Shock Wave Diffraction from Curved Surfaces," *Proceedings of the 15th International Symposium on Shock Waves and Shock Tubes*, Stanford Univ. Press, Bekerley, CA, 1985.

[14]Yang, J.Y., "Higher-Order Upwind Flux Difference Splitting Schemes for the Euler Equations Using Upstream Interpolations," *Notes on Numerical Fluid Mechanics*, Vieweg, Braunschweig/Wiesbaden, Vol. 10, (Proceedings of the 6th GAMM Conference on Numerical Methods in Fluid Mechanics, Göttingen, FRG), 1985, pp. 391–398.

[15]Anderson, W.K., Thomas, J.L., and van Leer, B., "A Comparison of Finite Volume Flux Vector Splittings for the Euler Equations," AIAA Paper 85-0122, 1985.